Co-phasing of the segmented mirror based on the generalized phase diversity wavefront sensor

Changwei Li [1, 2], Sijiong Zhang [1, 2 *]
[1]National Astronomical Observatories / Nanjing Institute of Astronomical Optics & Technology, Chinese Academy of Sciences, Nanjing 210042, China
[2]Key Laboratory of Astronomical Optics & Technology, Nanjing Institute of Astronomical Optics & Technology, Chinese Academy of Sciences, Nanjing, 210042, China

ABSTRACT

The stochastic parallel gradient descent algorithm based on the generalized phase diversity wavefront sensor is presented for co-phasing of segmented mirrors. Cost functions of the optimization algorithm were built up in different circular zones for intensity images of the sensor. In order to achieve high accuracy for co-phasing, four phase diversity functions with increasing amplitudes were applied to the sensor for improving the strength of output signal from the wavefront sensor during the aberrations of the segmented mirror decreasing with the co-phasing process. A simulated segmented mirror was used to test the feasibility of this method. The numerical experiments show that the co-phasing accuracy is very high for the aberrations of the segmented mirrors less than 1.5 wavelengths. And the algorithm is very robust and noise tolerant.

Keywords: Co-phasing; segmented mirror; wavefront sensing; optimization algorithm

1. INTRODUCTION

It is well known that telescopes with larger apertures are more sensitive to dim objects so that the deep space can be observed. That is why apertures of telescopes are designed larger and larger for the next generation of ground-based telescopes. Generally, there are two types of primary mirror for fabrication of telescopes. One is a monolithic primary mirror, and the other is a segmented one. For the next generation of telescopes with apertures much larger than 8 m, it is not practical and affordable to build telescopes with monolithic primary mirrors. Thus, a large telescope with many segmented mirrors is considered as a more preferable way. However, segmented mirrors could not provide a high quality image equivalent to that of a monolithic mirror unless co-phasing of the segmented mirrors is achieved. The procedure of co-phasing a segmented mirror is the process of removing misalignments, which result from relative piston aberrations between segments and tip/tilt aberrations of each segment. In order to eliminate aberrations caused by misalignments, several techniques have been developed by taking different optical methods, including wavefront sensing techniques [1, 2], phase diversity techniques [3, 4], diffraction techniques [5], interferometric techniques [6-8], and so on. Even though, co-phasing with high accuracy is difficult to achieve for segmented mirrors. A wavefront sensor was proposed based on generalized phase diversities (GPD) in 2004 [9]. This sensor, a null sensor for an undistorted input wavefront, is very simple and highly sensitive to both relative piston and tip/tilt aberrations for continuous and discontinuous input distorted wavefront.

Here, the GPD sensor is proposed to achieve co-phasing using stochastic parallel gradient descent algorithm (SPGD). Cost functions of the SPGD algorithm are built up in different circular zones for intensity images of the sensor to decouple the entangled effect between segments in different regions. Co-phasing with high accuracy was achieved by employing four diversity functions with increasing amplitudes. In order to test the feasibility and practicality of this method, a segmented mirror with 18 segments is used in the case of intensity images obtained from the sensor with and without random white Gaussian noise.

* sjzhang@niaot.ac.cn; phone +86 25 85482209; www.niaot.ac.cn.

Modern Technologies in Space- and Ground-based Telescopes and Instrumentation II,
edited by Ramón Navarro, Colin R. Cunningham, Eric Prieto, Proc. of SPIE Vol. 8450, 84500B
 · doi: 10.1117/12.923645

2. THEOTY OF THE GPD SENSOR

Figure 1 shows the schematic diagram of the GPD sensor. A deformable mirror is used to generate phase diversity functions. $\varphi(x,y)$ is the distorted wavefront, $\Phi(\xi,\eta)$ the Fourier Transform of the wavefront $\varphi(x,y)$, and the error signal $d(x,y)$ the difference between intensity images I_+ & I_- (I_+ & I_- are images with positive and negative phase diversity functions, respectively). The error signal could be expressed as [9]:

$$\begin{aligned} d(x,y) &= \left|\mathcal{F}\left\{\Phi(\xi,\eta)\cdot\exp(+i2\pi\phi_d)\right\}\right|^2 - \left|\mathcal{F}\left\{\Phi(\xi,\eta)\cdot\exp(-i2\pi\phi_d)\right\}\right|^2 \\ &= \left|\varphi(x,y)*\mathcal{F}\left\{\exp(+i2\pi\phi_d)\right\}\right|^2 - \left|\varphi(x,y)*\mathcal{F}\left\{\exp(-i2\pi\phi_d)\right\}\right|^2 \end{aligned} \tag{1}$$

where $\mathcal{F}$ is the operation of Fourier Transform, $*$ the operation of convolution, and ϕ_d a phase diversity function.

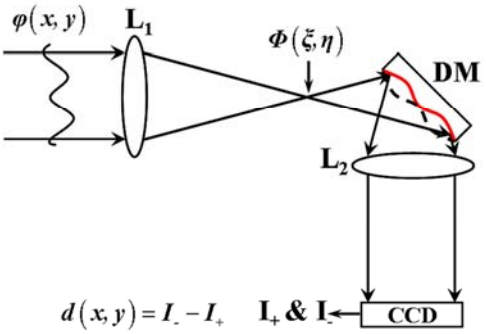

Figure.1 The schematic diagram of the GPD sensor.

Note that the error signal shows details of the input wavefront by the operation of convolution. The error signal of the GPD sensor could not be zero unless the input wavefront is an undistorted plane. Additionally, the error signal is mostly dependent on the phase diversity function. In order to get error signals with higher SNR, it is an effective way to increase the amplitude of the phase diversity function.

3. THE SPGD OPTIMIZATION ALGORITHM

The SPGD algorithm, which does not require wavefront sensing, is widely used in high resolution wavefront control [10, 11]. That is to say, systems can be optimized using this SPGD algorithm without the prior information of systems.

A cost function $J(\boldsymbol{u})$, which is a function of control parameters $\boldsymbol{u}=\{u_1,\cdots u_j,\cdots u_N\}$, is used to evaluate the performance of the optimization algorithm. N is the total number of the control channels. Small perturbations are generated and applied simultaneously to all control channels. The updated rule for all control channels could be given as:

$$u_j^{(n+1)} = u_j^{(n)} + \gamma\delta J^{(n)}\delta u_j^{(n)}, \tag{2}$$

where n is the number of iterations, γ a gain coefficient, $\delta u_j^{(n)}$ small perturbation for the j^{th} channel in the n^{th} iteration, and $\delta J^{(n)} = \delta J_+^{(n)} - \delta J_-^{(n)}$ the gradient estimation. Here, the optimal direction is dependent on the gain coefficient. Cost functions are optimized to maximum for positive sign, and vice versa. Oscillations of cost functions mostly resulted from larger amplitudes of perturbations.

Generally, small perturbations generated in the SPGD algorithm have identical amplitudes with a Bernoulli distribution. However, the statistical correlation of amplitudes of small perturbations may result in a decrease in the number of effective control channels [11]. In order to increase the number of effective control channels, small perturbations with random amplitudes in a specific range are used in the SPGD algorithm for co-phasing of segmented mirrors.

4. SIMULATION RESULTS AND DISSCUSSIONS

As shown in figure 2, a simulated mirror with 18 segments is taken as an example to test the feasibility and sensitivity of the co-phasing method. A segmented input wavefront of the mirror with peak to valley value of 1.46 waves will be

adjusted to a plane using the proposed co-phasing method. The procedure of co-phasing will be carried out with and without the existence of noise.

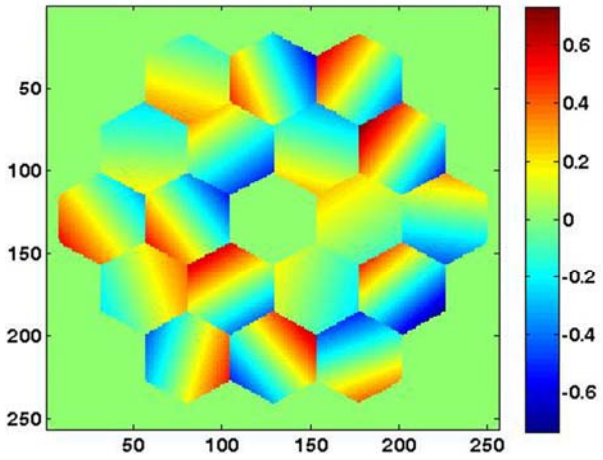

Figure 2. A simulated mirror with 18 segments.

4.1 Co-phasing without noise

The segmented wavefront, which is generated by the simulated mirror, is taken as an input to the GPD sensor. In the case of the defocus diversity function with a PV value of 0.62 waves, the error signal of the GPD sensor is shown in figure 3. In figure 3, the hexagonal array of the segmented wavefront can be clearly seen. It is easy to extract the hexagonal array of the segmented wavefront by image processing. The hexagonal array, the arrangements of each segment, is the only information needed for co-phasing segmented mirrors in our proposed method. After getting the hexagonal array of the whole mirror, co-phasing could be started to carry out.

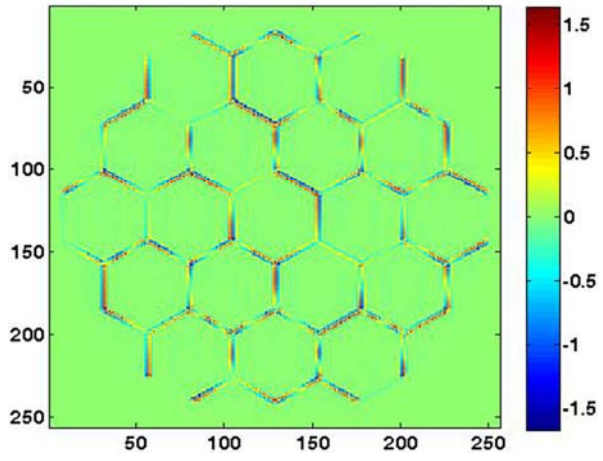

Figure 3. The error signal of the GPD sensor.

Before co-phasing control parameters and the cost functions of the SPGD optimization algorithm must be defined. Each segment has three degrees of freedom, one for relative piston, and the other two for tip/tilt. Thus, there are 54 parameters to control for co-phasing the segmented mirror. Cost functions defined in different circular zone are expressed as:

$$J_i = \sum \left[\left| \left(I_{+(Mea)} - I_{+(Cal)} \right) \cdot \mathrm{Cir}_i \right|^2 + \left| \left(I_{-(Mea)} - I_{-(Cal)} \right) \cdot \mathrm{Cir}_i \right|^2 \right], \tag{3}$$

where the subscripts *Mea* and *Cal* are intensity images measured and calculated respectively, Cir_i, built up on intensity images I_+ and I_-, is the circular zone. The circular zones, in which cost functions are defined on the intensity image I_+, are shown in figure 4.

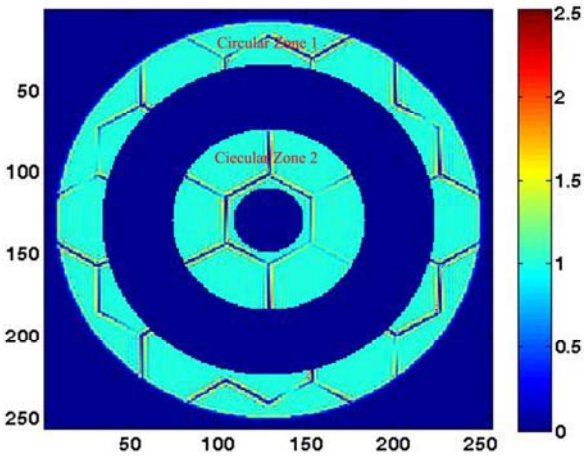

Figure 4. Circular zones built on the intensity image I+.

Once cost functions are defined, the solution of control channels could be updated according to equation 2. The gain coefficient in equation 2 is replaced by a variable one, which is changed with the iteration number:

$$\gamma^{(n+1)} = \gamma \Big/ (C+n)^{\alpha}, \qquad (4)$$

where C, α are constants.

The procedure of co-phasing is shown in figure 5. The procedure of co-phasing in different circular zones is designed to decouple the entangled effect between segments in different regions. Procedure in the whole mirror is intended to diminish the misalignments between different regions.

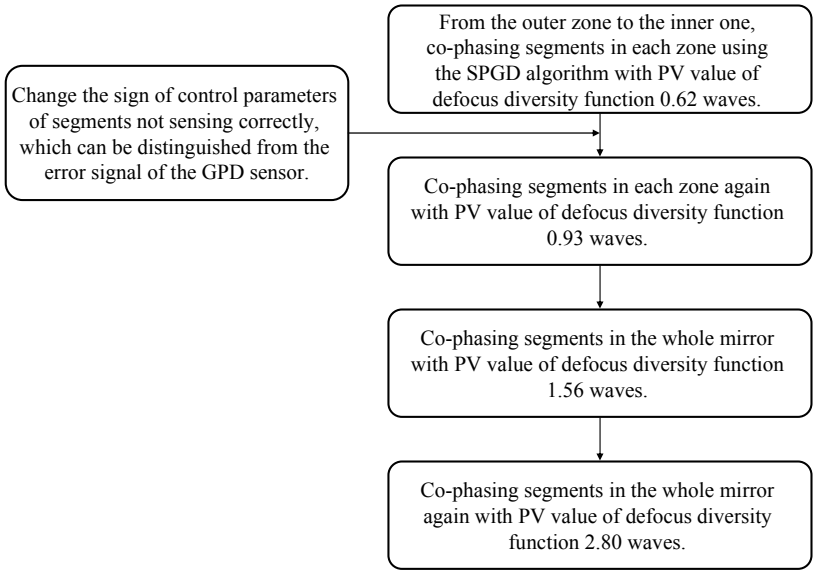

Figure 5. The procedure of co-phasing of segmented mirrors.

After optimizing with four diversity functions, the procedure of co-phasing is finished. The final results of co-phasing are shown in figure 6. Figure 6(a) shows the residual phase of the segmented wavefront. The PV value of the residual phase is 0.007 waves, which means co-phasing with high accuracy was achieved. As shown in figure 6(b), a cross section of the retrieved phase profile fits that of the initial phase surprisingly well. The evolution of cost functions is shown in figure 6(c). As the change of the cost function is extremely slow exceeding the number of iteration 4500, a break was inserted from iteration number 4500 to 21000 to display cost functions more detail. In figure 6(c), there are four peaks including the maximum. All of the peaks are resulted from the increments of the amplitudes of defocus diversity functions and the change of circular zones built up on the intensity images.

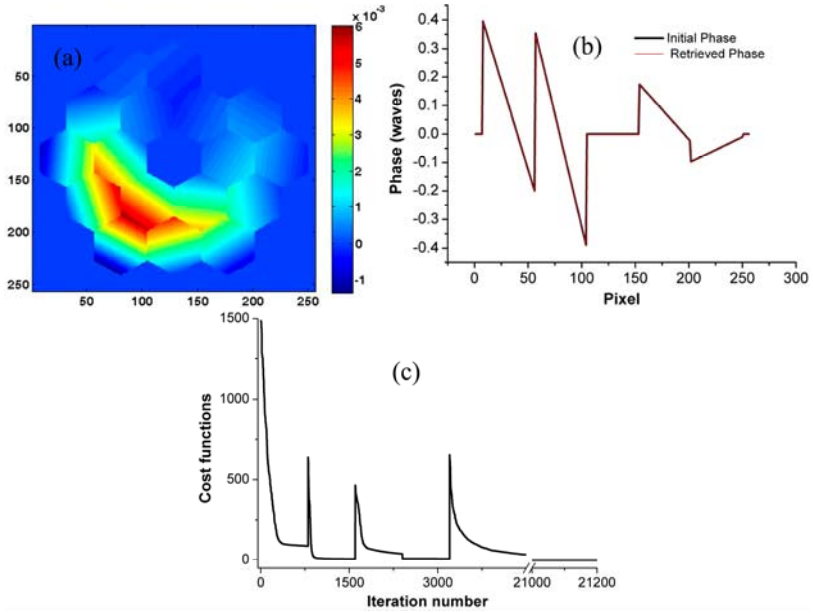

Figure 6. (a) The residual phase of the segmented wavefront after co-phasing; (b) a cross section of the retrieved phase profile fits that of the initial phase; (c) cost functions evolved with the number of iterations.

4.2 Co-phasing with a noise

In order to examine the practicality of the co-phasing method, a random white Gaussian noise is introduced to intensity images (I_+ & I_-) of the GPD sensor. According to Ref 12, the SNR is defined as what follows:

$$SNR = \frac{\left|\overline{I_{\pm}}\right|}{\sigma}, \qquad (5)$$

where $I_{\pm}$ is the intensity images, σ the variance of noise introduced to the sensor.

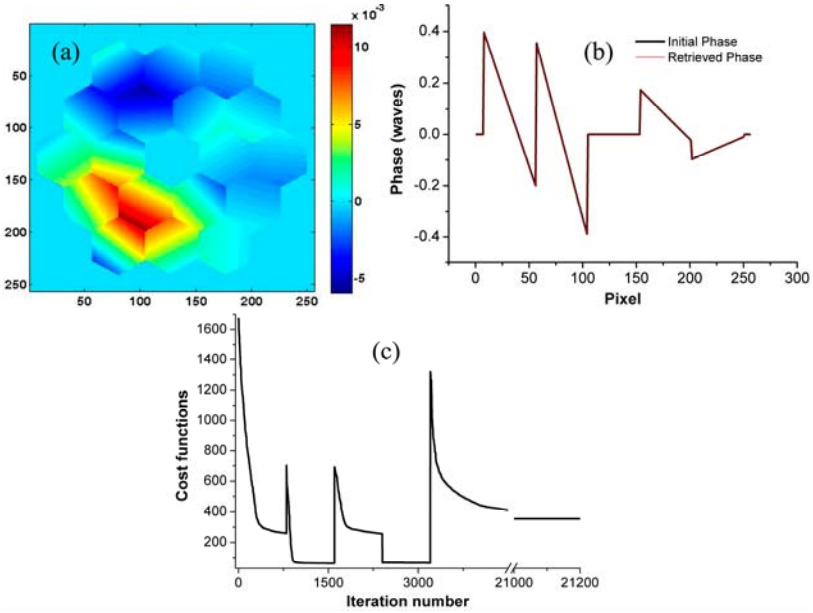

Figure 7. (a) The residual phase after co-phasing with a noise; (b) a cross section of retrieved phase profile fits that of the initial phase; (c) cost functions evolved with the number of iterations.

After introducing a noise to the sensor, the same segmented input wavefront is used to the GPD sensor. Repeat the procedure of co-phasing again. The final results of co-phasing with a noise of SNR = 20 is shown in figure 7. Figure 7(a) shows the residual phase of the segmented wavefront, the PV value of which is 0.017 waves. Although the PV value of the residual phase increases more than two times, the precision of co-phasing is still high. A cross section of retrieved phase profile is in good agreement with that of the initial phase, as shown in figure 7(b). Cost functions evolve with the iteration number is shown in figure 7(c). Obviously, the minimum of cost functions are much greater than that without noise. Even though, the final results of co-phasing with noise show that co-phasing with high accuracy was achieved in the existence of noise.

5. CONCLUSIONS

A new method for co-phasing segmented mirrors is presented, which is based on the GPD wavefront sensor using the SPGD optimization algorithm. Co-phasing with high accuracy has been achieved by increasing the amplitude of defocus diversity function and building up cost functions in different circular zones to decouple the entangled effect for segments in different regions. The numerical experiments show that the proposed method is highly sensitive and noise tolerant. Our future work will be concentrated on experimental verification of this co-phasing algorithm in laboratory.

6. ACKNOWLEDGEMENTS

This work is supported by the dedicated operation funding for astronomical observation stations and facilities from the Chinese Academy of Sciences (CAS).

REFERENCES

[1] Orlov, V. G., Cuevas, S., Garfias, F., Voitsekhovich, V. V., and Sanchez, L. J., "Co-phasing of segmented mirror telescopes with curvature sensing," Proc. SPIE 4004, 540-551 (2000).
[2] Esposito, S., and Devaney, N., "Segmented telescopes co-phasing using Pyramid Sensor," Proc. ESO Conference and Workshop 58, 161-166 (2002).
[3] Paxman, R., and Fienup, J., "Optical misalignment sensing and image reconstruction using phase diversity," JOSA A 5, 914-923 (1988).
[4] Kendrick, R. L., Acton, D. S., and Duncan, A., "Phase-diversity wave-front sensor for imaging systems," Applied Optics 33, 6533-6546 (1994).
[5] Chanan, G., Ohara, C., and Troy, M., "Phasing the mirror segments of the Keck telescopes II: the narrow-band phasing algorithm," Applied Optics 39, 4706-4714 (2000).
[6] Pizarro, C., Arasa, J., Laguarta, F., Tomàs, N., and Pinto, A., "Design of an interferometric system for the measurement of phasing errors in segmented mirrors," Applied Optics 41, 4562-4570 (2002).
[7] Wilhelm, R., Luong, B., Courteville, A., Estival, S., Gonté, F., and Schuhler, N., "Dual-wavelength low-coherence instantaneous phase-shifting interferometer to measure the shape of a segmented mirror with subnanometer precision," Applied Optics 47, 5473-5491 (2008).
[8] Yaitskova, N., Dohlen, K., Dierickx, P., and Montoya, L., "Mach-Zehnder interferometer for piston and tip-tilt sensing in segmented telescopes: theory and analytical treatment," JOSA A 22, 1093-1105 (2005).
[9] Campbell, H. I., Zhang, S., Greenaway, A. H., and Restaino, S., "Generalized phase diversity for wave-front sensing," Optics letters 29, 2707-2709 (2004).
[10] Weyrauch, T., Vorontsov, M. A., Bifano, T. G., Hammer, J. A., Cohen, M., and Cauwenberghs, G., "Microscale adaptive optics: wave-front control with a μ-mirror array and a VLSI stochastic gradient descent controller," Applied Optics 40, 4243-4253 (2001).
[11] Vorontsov, M., and Sivokon, V., "Stochastic parallel-gradient-descent technique for high-resolution wave-front phase-distortion correction," JOSA A 15, 2745-2758 (1998).
[12] Roggemann, M. C., Tyler, D. W., and Bilmont, M. F., "Linear reconstruction of compensated images: theory and experimental results," Applied optics 31, 7429-7441 (1992).